Mechatronics 39 (2016) 63–76

Contents lists available at ScienceDirect

Mechatronics

journal homepage: www.elsevier.com/locate/mechatronics

Experimental and theoretical study of semi-active friction tendons

Hernán Garrido, Oscar Curadelli*, Daniel Ambrosini

National University of Cuyo, CONICET, Eng. Faculty, Mendoza, Argentina

ARTICLE INFO

Article history:
Received 20 April 2015
Revised 12 July 2016
Accepted 15 August 2016

Keywords:
Vibration control
Semi-active control
Friction dissipation
Cable slackening
Velocity-feedback
Force-feedback

ABSTRACT

For purposes of mitigating vibrations, a Semi-Active Friction Tendon (SAFT), which consists of a semi-active friction damper and an auxiliary spring that are linked to the structure by a cable, is studied experimentally, numerically and analytically. Two semi-active control laws are implemented, one is based on velocity-feedback (denoted as SQDCL) and the other is based on force-feedback (denoted as SPCL); the passive control case is also studied for comparison. From the assessment of system displacement and hysteretic behaviour of SAFTs two main conclusions are drawn. First, the effectiveness of the optimized passive-control case can always be improved by using semi-active control with any of the studied control laws. Second, the SPCL is more effective for large displacements, while the SQDCL is more advantageous for very small displacements. Moreover, closed-form expressions for the dissipated energy are derived for the three cases under consideration. These expressions can be used in preliminary design of SAFTs to compare with other alternatives, to decide between passive and semi-active control, and to choose the more suitable control law.

1. Introduction

Vibrations can be problematic in different types of structures (either civil, mechanical, aerospace, industrial, home appliances, etc.); namely, they can cause discomfort in people due to floor vibration [1] or ambient noise [2], malfunctioning of sensitive instruments [3,4], structural deterioration [5], and, in some cases, even collapse.

To mitigate the problem of structural vibrations, many methodologies have been proposed [6] and implemented in real cases [7,8]. These can be classified into four types of control: (1) passive control (PC), which uses constant-parameters devices to dissipate energy [7]; (2) active control (AC), which uses actuators capable of exerting forces on the structure [1,9–12]; (3) semi-active control (SAC), which uses devices whose parameters are "smartly" adjusted in real-time [2,13–19]; and (4) Hybrid Control (HC), combining two or three of the other types of control [20]. SAC is attractive because, in general, it is more effective and robust against parameter variation than PC and it requires much less power to operate than AC [16].

Regardless of the type of control, the mechanical connection of control devices to the structure is of extreme importance because of its influence in the effectiveness of the control system. In particular, if the structure is very slender, or because of architectural restrictions, the use of traditional braces can become impractical. An appropriate mechanical arrangement that includes pre-tensioned cables is a possible alternative solution. Besides, in large space structures [21], in which weight and volume must be reduced and the structural elements have to be deployable, the use of this kind of linkages is advantageous and widely accepted [22]. The key issue, mainly in PC systems, is a suitable cable pre-tension to avoid undesirable events as sudden pulls, poor performance and eventually disabling of damper due to cable slackening.

There are some examples of passive vibration control systems that use cables in the literature. For instance, in [23] it is shown the control of a chimney by using a cable in series with a passive friction damper. To mitigate the seismic response of a steel building, Pekcan et al. [24] experimentally studied a PC system using elastomeric spring dampers and fuse-bars, both linked to a real structure building through a cable. In the same context, Mualla and Belev [25] considered the linking of a passive friction damper using two bars that can be pre-tensioned to prevent its buckling. Currently, this friction damper is commercialized by Damptech to be used in buildings and bridges.

In order to provide damping to structures using AC, the linkage of hydraulic or piezoelectric actuators by means of cables has been addressed by many researchers [5,26–28]. Recently, Wang et al. [29] considered the incorporation of PZT actuators into flexible cables belonging to a cable net structure for an active adjustment of its shape. For an extensive review on active cable and tendon control, see [30].

* Corresponding author at: Facultad de Ingeniería, Centro Universitario, Parque Gral. San Martín, (5500) Mendoza, Argentina.
E-mail address: ocuradelli@fing.uncu.edu.ar (O. Curadelli).

http://dx.doi.org/10.1016/j.mechatronics.2016.08.005
0957-4158/

In the context of SAC applied to cable-linked dampers, Klein and Healey [31] proposed the coupling of two buildings with cables that could be released and tightened to provide specified dissipative control forces. Erramouspe et al. [32] studied a semi-active damper using two pre-tensioned cables, in order to implement a resetting stiffness controller. In a recent work [33], it was proposed a device named Semi-Active Friction Tendon (SAFT) for the vibration control of space structures (requiring only one cable per damper) which consists of a friction damper in parallel with an auxiliary spring, both linked to the structure by means of a cable. SAFTs can operate with PC, or with SAC. The behaviour of the SAFT with SAC was studied using two types of control laws: (1) the Simplified Quickest Descent Control Law (SQDCL), based on velocity-feedback; or (2) the Slackening Preventing Control Law (SPCL), based on force-feedback [33]. It was demonstrated through nonlinear numerical simulations that SAC can be superior to PC in terms of both: structural response reduction (effectiveness) and robustness against loss of pre-tension (reliability). Thus, the benefits of cable linkage and the high energy dissipation capacity and simplicity of friction dampers can be used to solve a wide variety of vibration problems as, for example: flexible and deployable space structures carrying sensitive equipment [21,22], chimney vibration [23], seismic response of buildings and works of art [24,34,35], and connection between neighbouring tall buildings to mitigate wind vibration [1].

Velocity-feedback has been largely used in vibration control since it is a natural approach to add damping to a structure [1]. In the case of SAFTs, velocity-feedback also has particular benefits related to the slackening issue. On the other hand, force-feedback has been used in AC and HC systems with some success [20,27]. In fact, there is a duality between integral force-feedback for displacement actuators (those whose stroke is proportional to its control signal) and direct velocity-feedback for force actuators [1]. In SAC systems, a force-feedback (inner) loop can be implemented to approximately generate a desired control force by means of variable damping [36]. Unlike these previous works, SAFTs can use force-feedback to explicitly deal with the cable-slackening issue.

In view of the above, the present paper studies numerically and experimentally the effectiveness of SAFTs with PC and SAC, under a control law based on velocity-feedback denoted as SQDCL and a control law based on force-feedback, denoted as SPCL. Hysteretic behaviour of SAFTs is analytically studied and compared to experimental and numerical results. Closed-form expressions for the energy dissipated per cycle are derived as functions of the system parameters and the maximum displacement. Since the enclosed area in a hysteresis loop represents the energy dissipated per cycle, and this energy is closely related to the effective damping [37], the comparison between area sizes of each hysteresis loop reveals the intrinsic damping characteristics of each case. The results derived in the present paper allow estimating expectable performance in different application cases, e.g. civil and mechanical structures (a specific application case of a real space structure was addressed through simulations in [33]).

2. Vibration control system based on SAFTs

As mentioned before, each SAFT consists of a friction damper in parallel with an auxiliary spring, in which one end is fixed to the reference frame, and the other end is in series with a cable which links the friction damper to the structure that is to be controlled (an extension of this model to multi-degree-of-freedom structures with multiple SAFTs in arbitrary configurations can be found in [33]). Thus, when the structure moves horizontally under lateral forces, the relative displacements between sliding pads of the damper produce a friction force that is proportional to the normal force on the interfaces, which dissipate energy and resist to the movement.

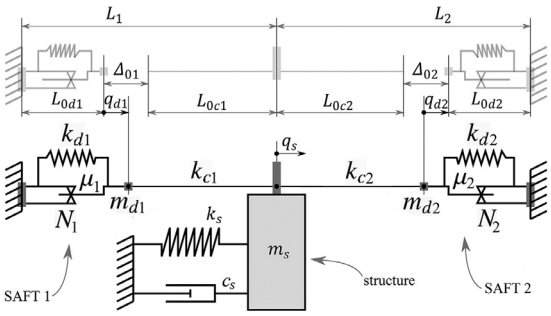

Fig. 1. Two SAFTs connected to a SDOF structure; grey lines indicate undeformed shape and black lines indicate pre-tensioned shape.

Fig. 1 schematically shows two SAFTs connected in opposition to a single-degree-of-freedom (SDOF) structure, indicating: displacement, mass, stiffness, and damping coefficient of the structure as q_s, m_s, k_s and c_s, respectively; displacement, mass, friction coefficient, and normal force of the ith friction damper as q_{di}, m_{di}, μ_i, and N_i, respectively; pre-tension displacement and stiffness of the ith auxiliary spring as Δ_{0i} and k_{di}, respectively; and tensile stiffness of the ith cable as k_{ci}. The constant parameter L_i is the final length of the ith SAFT in static pre-tensioned state; whereas L_{0ci} and L_{0di} are the natural lengths (without pre-tension) of the cable and auxiliary spring, respectively, of the ith SAFT.

The SAFTs can operate with two types of control: (1) PC, where N_i is constant during the operation; and (2) SAC, where N_i is continuously adjusted during the operation by a predefined control law.

2.1. Nonlinear model

The equations of motion for the system shown in Fig. 1 can be stated as [33]:

$$m_s\ddot{q}_s(t) + c_s\dot{q}_s(t) + k_sq_s(t) + F_{c1}(t) - F_{c2}(t) = F_{es}(t), \tag{1}$$

$$m_{d1}\ddot{q}_{d1}(t) + k_{d1}q_{d1}(t) + F_{f1}(t) - F_{c1}(t) = F_{ed1}(t), \tag{2}$$

$$m_{d2}\ddot{q}_{d2}(t) + k_{d2}q_{d2}(t) + F_{f2}(t) + F_{c2}(t) = F_{ed2}(t), \tag{3}$$

where: t is the time, F_{es}, F_{ed1} and F_{ed2} are external forces applied to the structure mass and to the SAFT masses; F_{c1} and F_{c2} are the cable forces; and F_{f1} and F_{f2} are the forces exerted by the friction dampers. It is assumed that both SAFTs are identical.

The pre-tension of the ith SAFT is defined in terms of an initial displacement Δ_{0i} as:

$$\Delta_{0i} = L_i - L_{0ci} - L_{0di}, \quad i = 1, 2. \tag{4}$$

Assuming that the cables display an elastic behaviour and can only exert tensile forces with constant stiffness, their corresponding tensile forces are given by the following equations:

$$F_{c1}(t) = k_{c1}\mathrm{sat}(q_s(t) - q_{d1}(t) + \Delta_{01}), \tag{5}$$

$$F_{c2}(t) = k_{c2}\mathrm{sat}(-q_s(t) + q_{d2}(t) + \Delta_{02}), \tag{6}$$

in which sat(·) is a saturation function defined as:

$$\mathrm{sat}(x) = \begin{cases} 0, & |x < 0 \\ x, & |x \geq 0 \end{cases}, \tag{7}$$

For PC, the normal force $N_i(t) = N$, i.e. constant over time. In the case of SAC, it is assumed that the normal force $N_i(t)$ of each

friction damper can be instantaneously adjusted between $N_{\min}$ and $N_{\max}$, which are design parameters of the friction dampers.

The friction force exerted by each damper can be expressed through the Coulomb's friction law as:

$$F_{fi}(t) = \mu_i N_i(t)\text{sign}(\dot{q}_{di}(t)),\ \ i = 1, 2, \tag{8}$$

in which: μ_i is the friction coefficient of the friction damper and sign(·) is the sign function as defined in [33]. While more refined friction models are available in the literature (e.g. Stribeck's, Dahl's and LuGre's models [38]), the Coulomb's model is used in this work because it is the simplest friction model that captures the dominant nonlinearity due to static friction.

2.2. Semi-active control laws

2.2.1. Simplified Quickest Descent Control Law (SQDCL)

In order to obtain, from the application of Lyapunov's Theory, a velocity-feedback control law which aims to reduce the total energy in the structure as quick as possible [14,39], the Simplified Quickest Descent Control Law (SQDCL) is stated as follows:

$$N_1(t) = \begin{cases} N_{\min}, & |\dot{q}_s(t) \le 0 \\ N_{\max}, & |\dot{q}_s(t) > 0 \end{cases}, \tag{9}$$

$$N_2(t) = \begin{cases} N_{\min}, & |\dot{q}_s(t) \ge 0 \\ N_{\max}, & |\dot{q}_s(t) < 0 \end{cases}. \tag{10}$$

SQDCL was developed in [33] from a Quickest Descent Control Law and then simplified after the assumption that the following conditions are satisfied most of the time:

$$\dot{q}_s(t) > 0 \rightarrow \dot{q}_{d1}(t) \ge 0, \tag{11}$$

$$\dot{q}_s(t) < 0 \rightarrow \dot{q}_{d2}(t) \le 0, \tag{12}$$

$$F_{ci}(t) > 0 \quad \forall t, i = 1, 2. \tag{13}$$

Briefly, Eqs. (11) and (12) state that, most of the time, the structure and each friction damper cannot move in opposite directions tending to tighten the cable. This assumption comes from the fact that the cable has a stiffness several times higher than the spring stiffness and the structure inertia is several times higher than damper inertia. For its part, Eq. (13) states that the cables are taut most of the time. That is, it is assumed that the friction force ($\mu N_i(t)$) is reduced (at the appropriate times) in such a way to be below the spring force ($k_{di}q_{di}(t)$), thus mitigating the cable slackening. Please refer to [33] for a detailed development of this control law, which includes the verification of the preceding assumptions.

2.2.2. Slackening Preventing Control Law (SPCL)

This force-feedback control law is obtained from a heuristic approach aiming to explicitly prevent the cable from slackening. By sensing the cable forces $F_{c1}(t)$ and $F_{c2}(t)$ through load cells, it is possible to mitigate the cable slackening by decreasing the normal force of each friction damper when the corresponding cable is not under tension; since the auxiliary spring can "pull" from the cable only if the friction force ($\mu_i N_i$) is smaller than the auxiliary-spring force ($k_{di}q_{di}$). This simple idea leads to the Slackening Preventing Control Law (SPCL) [33], which, considering the offset drift in load-cells, is stated as:

$$N_i(t) = \begin{cases} N_{\min}, & F_{ci}(t) \le v_F \\ N_{\max}, & F_{ci}(t) > v_F \end{cases},\ \ i = 1, 2. \tag{14}$$

The parameter v_F is a force threshold below which the cable is considered slack. This must be greater than the maximum expectable offset error in force measuring, and as small as possible, in order to maximize the effectiveness (as it is shown in Section 3).

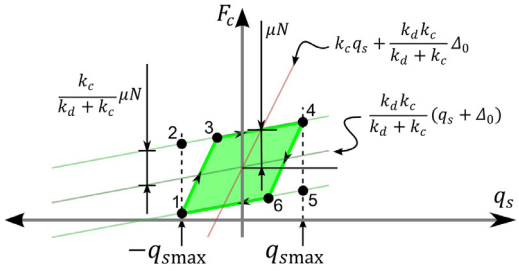

Fig. 2. Analytical construction of hysteresis loop with PC.

3. Hysteretic behaviour of a SAFT

The usability of any damping-based vibration control method strongly depends on the application case, i.e.: required damping/energy dissipation, stringency of vibration limits, geometrical and physical constraints and technological aspects. In this context, the hysteretic behaviour of damping devices could be used in first instance to compare different alternatives of vibration control. In this section, the hysteretic behaviour of a SAFT is analytically investigated. The expressions presented in this section allow predicting the relative performance of different alternatives, which is then validated through experimental tests and numerical simulations in Sections 5 and 6.

Analytical constructions of hysteresis loops (i.e. the relations between q_s and F_c) are made neglecting the external- and inertial-forces on friction dampers, and assuming that the structure imposes a cyclic displacement with constant amplitude, on the SAFT. Such a simplified model is obtained by combining Eq. (2) with Eq. (8), and recalling Eq. (5) under the assumption that the cable is always taut (i.e. $F_c(t) > 0\,\forall t$), which yields:

$$k_d q_d(t) + \mu N(t)\text{sign}(\dot{q}_d(t)) = F_c(t), \tag{15}$$

$$F_c(t) = k_c(q_s(t) - q_d(t) + \Delta_0). \tag{16}$$

The branches that comprise the hysteresis loops can be constructed by combining Eqs. (15) and (16); namely: the *loading branch* is obtained by making $\text{sign}(\dot{q}_d(t)) = 0$ and $\text{sign}(\dot{q}_s(t)) = 1$; the *unloading branch* is obtained by making $\text{sign}(\dot{q}_d(t)) = 0$ and $\text{sign}(\dot{q}_s(t)) = -1$, the *forward-friction branch* is obtained by making $\text{sign}(\dot{q}_d(t)) = 1$, and the *backward-friction branch* is obtained by making $\text{sign}(\dot{q}_d(t)) = -1$.

3.1. Passive control

From Eqs. (15) and (16), and considering that $N(t)$ is actually a constant equal to N, the stable hysteresis loop shown in Fig. 2 can be constructed. The main characteristics of the hysteresis loop are: (1) the forward-friction branch (3-4) is symmetric to the backward-friction branch (6-1), being both equally dependent on N; and (2) both, the loading and unloading branches (1–3 and 4–6), have a slope approximately equal to the cable stiffness k_c.

Under constant-amplitude cyclic displacement, a sufficient condition for the cable to be always taut can be inferred by considering the limit case in which point (1) of Fig. 2 lies in the q_s-axis. Thus, substituting $q_s = -q_{s\max}$, $\dot{q}_d < 0$ and $F_c = 0$ into Eqs. (15) and (16) leads to the following taut-cable condition:

$$\mu N \le k_d(\Delta_0 - q_{s\max}), \tag{17}$$

To ensure that the cable gets taut at least once in every cycle, even in the likely case in which the successive cycles have decreasing maximum displacements, a sufficient condition can be inferred

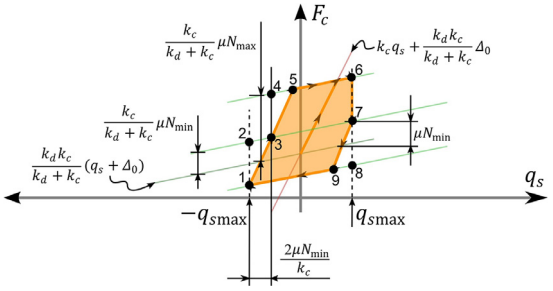

Fig. 3. Analytical construction of a hysteresis loop with SAC and the SQDCL.

by considering the limit case in which the cable gets slack during the backward-friction branch at zero displacement. Thus, substituting $q_s = 0$, $\dot{q}_d < 0$ and $F_c = 0$ into Eqs. (15) and (16) yields the following taut-cable condition:

$$\mu N \le k_d \Delta_0, \tag{18}$$

In the Appendix it is shown that, for large displacements, the following general expression approximates the energy dissipated per cycle when using PC:

$$E_{D(PC)} \approx \begin{cases} 4q_{smax}\mu N & \text{if } \mu N < k_d(\Delta_0 - q_{smax}) \\ 2q_{smax}\mu N + 2\mu N\Delta_0 & \text{if } k_d(\Delta_0 - q_{smax}) \\ \quad -\dfrac{2(\mu N)^2}{k_d} & \le \mu N < k_d\Delta_0 \end{cases} \tag{19}$$

As expected, the first piece of Eq. (19) reduces to the standard result of Coulomb's friction law [23] and $E_{D(PC)}$ is independent of cable stiffness but is strongly affected by cable slackening since a detrimental effect ($-\frac{2(\mu N)^2}{k_d}$) appears when condition (17) is not satisfied.

On the other hand when displacements are very small, cable stiffness plays an important role on the energy dissipated since it defines the maximum displacement below which there is no energy dissipated by the following expression (Appendix, Eq. A.4):

$$E_{D(PC)} = 0 \text{ if } q_{smax} \le \frac{\mu N}{k_c}, \tag{20}$$

In the most favourable case in which condition (17) is satisfied, the dissipated energy $E_{D(PC)}$ given by Eq. (19) can be increased by augmenting the normal force N. However, this sacrifices performance at small displacements, because the lower bound on the maximum displacement with dissipation of energy, given by Eq. (20), is also increased.

3.2. Semi-active control

3.2.1. Simplified Quickest Descent Control Law (SQDCL)

From Eqs. (15) and (16), and considering that $N(t)$ is equal to $N_1(t)$ in Eq. (9), the stable hysteresis loop shown in Fig. 3 can be constructed for SAC with the SQDCL. Two aspects are worth mentioning: (1) the enclosed area can be increased upward by increasing N_{max}, without modifying the backward-friction branch (9-1); and (2) the unloading branch (6-7-9) has an abrupt drop (6-7) showing a phenomenon commonly known as resetting stiffness [31,32,40,41], which stands out for a suddenly elastic energy dissipation. In this case, the cable stiffness acts as the resettable stiffness and the friction damper acts as the releasing mechanism.

By inspecting Fig. 3 and with a similar argument to that of PC, it can be inferred the following condition for the cable to be always taut:

$$\mu N_{min} \le k_d(\Delta_0 - q_{smax}). \tag{21}$$

and it can be ensured that the cable gets taut at least once in every cycle if:

$$\mu N_{min} \le k_d \Delta_0, \tag{22}$$

even in the likely case in which the successive cycles have decreasing maximum displacements. It is worth noting that, unlike taut-cable conditions (17) and (18) (PC), conditions (21) and (22) only depend on the design parameter N_{min}. For this reason, SAC under the SQDCL should be more robust against loss of pre-tension than PC.

In the Appendix, Eq. (A.13) shows that, for large displacements in which the deformation of cable can be negligible, the energy dissipated per cycle with SQDCL can be approximate by:

$$E_{D(SQDCL)} \approx 2q_{smax}(\mu N_{max} + \mu N_{min}) \text{ if } \mu N_{min} < k_d(\Delta_0 - q_{smax}). \tag{23}$$

When comparing Eqs. (23) and (19), it is observed that $E_{D(SQDCL)} < E_{D(PC)}$ if the cable is taut and $N = N_{max}$. However, N_{max} can be chosen much larger than N, still avoiding cable slackening, in such a way that $E_{D(SQDCL)} \gg E_{D(PC)}$. For this reason, SAC under the SQDCL should be more effective than with PC.

As in the case of PC, cable stiffness influences the performance at very small displacements, since (see, Appendix, Eq. (A.12)):

$$E_{D(SQDCL)} = 0 \text{ if } q_{smax} \le \frac{\mu N_{min}}{k_c}, \tag{24}$$

Unlike the case of PC, the dissipated energy $E_{D(SQDCL)}$ given by Eq. (23) can be increased as desired by means of the design parameter N_{max} without sacrificing performance at small displacements, i.e. without increasing the lower bound on the maximum displacement with zero dissipation of energy (Eq. 24), since this latter only depends on N_{min}.

3.2.2. Slackening Preventing Control Law (SPCL)

From Eqs. (15) and (16), and considering that $N(t)$ is equal to $N_1(t)$ in Eq. (14), hysteresis loops can be constructed for SAC with the SPCL. As in the previous case, taut-cable conditions (21) and (22) remain. Since hysteresis loops stabilize after many cycles, it is convenient to address the cases of large displacements and those of very small displacements separately.

When the maximum displacement is large enough and $k_c \gg k_d$, three characteristic cases stand out depending on the maximum normal force N_{max}, for given values of $k_d\Delta_0$, q_{smax}, and v_F (Fig. 4(a–c)). Thus, as shown in the Appendix, (Eq. A.14), the energy dissipated per cycle is approximated as follows:

$$E_{D(SPCL)} \approx \begin{cases} 4\mu N_{max} q_{smax} & \text{if } \mu N_{max} \le k_d(\Delta_0 - q_{smax}) - v_F, \\ 2q_{smax}(\mu N_{max} + k_d\Delta_0 - v_F) & \text{if } \mu N_{max} \ge k_d(\Delta_0 + q_{smax}) - v_F, \\ 4\mu N_{max} q_{smax} & \text{elsewhere} \\ \quad -\dfrac{(\mu N_{max} - k_d(\Delta_0 - q_{smax}) + v_F)^2}{2k_d} & \\ \text{if } \mu N_{min} < k_d(\Delta_0 - q_{smax}) - v_F. \end{cases} \tag{25}$$

When comparing Eqs. (25) and (23) and taking into account that v_F is very small and $k_d\Delta_0 > \mu N_{min}$, it is observed that $E_{D(SQDCL)} < E_{D(SPCL)}$ which means that higher performance is expected from SPCL than from SQDCL for large displacements.

Regarding performance at very small displacements, the Eq. (A.15) in the Appendix, shows from Fig. 5 that:

$$E_{D(SQDCL)} = 0 \quad \text{if} \quad q_{smax} \le \frac{\mu N_{max} + k_d\Delta_0 - v_F}{k_c}, \tag{26}$$

By comparing Eqs. (26) and (25), it is inferred that SPCL has the same disadvantage that PC, i.e. it is impossible to improve performance at large displacements without sacrificing performance at

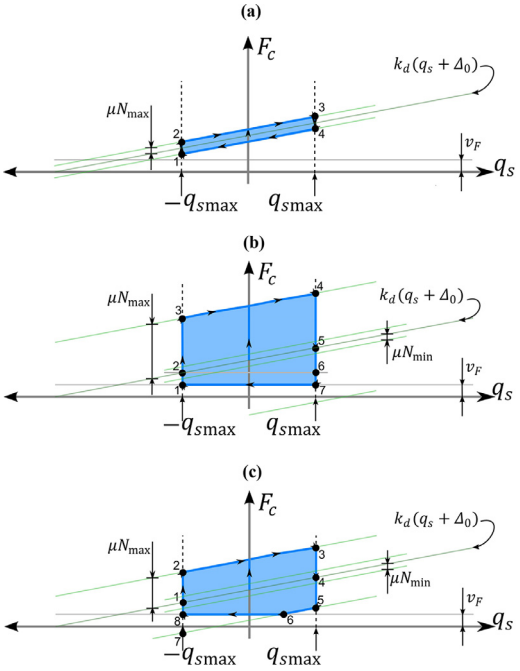

Fig. 4. Analytical construction of hysteresis loops with SAC and the SPCL, for large displacements.

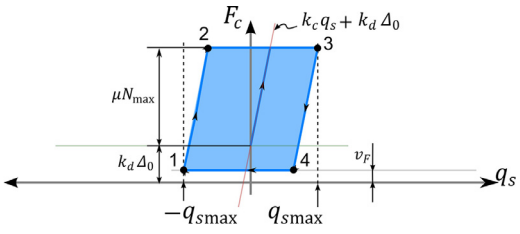

Fig. 5. Analytical construction of a hysteresis loop with SAC and the SPCL, for very small displacements.

small displacements because both depend on the same design parameters. The only alternative is to increase cable stiffness, which evidently has practical limitations.

4. Experimental setup

In order to assess the performance of a structure controlled by two opposing SAFTs with PC and SAC, shaking table tests were carried out by using the experimental setup shown in Fig. 6(a) and schematized in Fig. 6(b).

4.1. Controlled structure

The controlled structure is a moment-resisting steel frame, which can be modelled by a single-degree-of-freedom (SDOF) system having the following parameters: mass $m_s = 41.98$ kg, stiffness $k_s = 4600$ Nm^{-1}, and internal damping ratio $\zeta_s = 0.79\%$; which were identified through free-vibration tests and curve fitting.

4.2. Measuring system

An optoNCDT1607-200 laser optical displacement sensor from MICRO-EPSILON with a resolution (noise) of 60 μm was used to measure the relative displacement between the top and the base of the structure. To measure the cable forces, one CZA-30 load

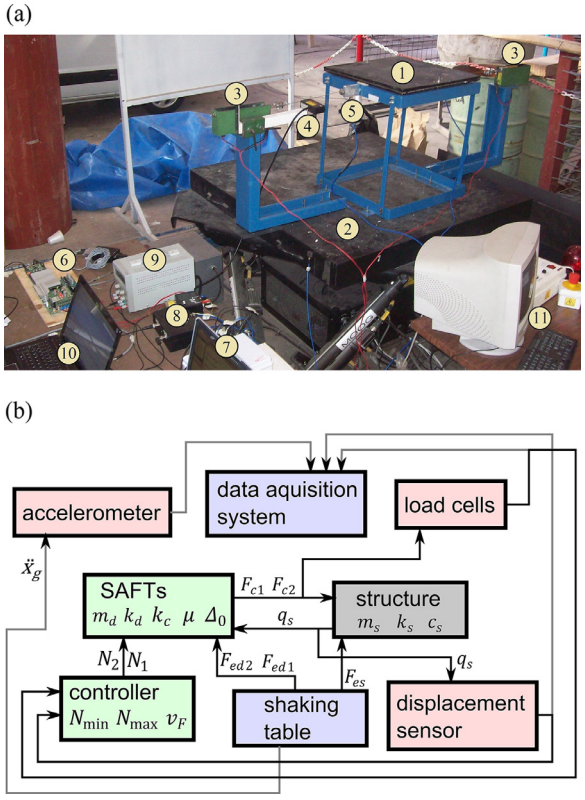

Fig. 6. Experimental setup. (a) General view: (1) structure to be controlled, (2) shaking table, (3) SAFTs, (4) displacement sensor, (5) load cell, (6) controller, (7) data acquisition system, (8) signal conditioners, (9) power supply, (10) personal computer used to setup the controller, and (11) personal computer used to command the shaking table. (b) Simplified block diagram.

cell from FLEXAR with a resolution of 0.1 N was installed in series with each cable. Output signals from the displacement sensor and load cells feed analog inputs of the controller (to implement the SQDCL and the SPCL, respectively) and the data acquisition system, which is based on a PCM-DAS16D/16 board from COMPUTERBOARDS and a personal computer. Base acceleration was also measured and recorded to be used as excitation in the numerical simulations.

4.3. Control system

Each SAFT is assembled with the following elements: (1) a friction damper built with three sliding steel pads in sandwich (see Fig. 7), whose normal force is generated by two 1300H electromagnetic actuators from CONTROLS COMPANY ARGENTINA S.A.I.C.; (2) an steel-coil auxiliary spring; and (3) a fibre-core steel twisted cable of 2 mm diameter (see Fig. 7). Before tests, the following parameters of the SAFT were experimentally identified: $m_d = 0.17$ kg, $k_d = 200$ Nm^{-1}, $k_c = 10,000$ Nm^{-1}, $\Delta_0 = 0.0387$ m ($k_d\Delta_0 = 7.74$ N). Since each damper has two steel friction interfaces, whose standard friction coefficient is 0.5, the friction coefficients were assumed as $\mu_1 = \mu_2 = \mu = 1$ from an estimation based on the experimental identification of μN. When the SPCL was used, the force threshold was set to $v_F = 1$ N.

The controller was based on a Digital Signal Controller (DSC) dsPIC33EP512MU810 from MICROCHIP in which the SQDCL and the SPCL were implemented separately. In the case of the SQDCL, the DSC is also used to estimate the sign of the structure velocity from displacement measurements by using the two-point finite difference method with a time step of 10 ms. The controller energizes the coil of each electromagnetic actuator through a

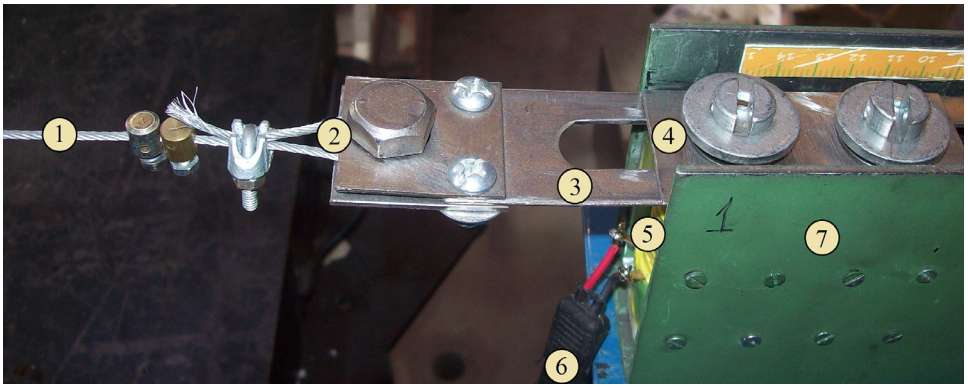

Fig. 7. Detail of a SAFT: (1) cable, (2) cable mechanical connection, (3) central pad of the friction damper, (4) external pad of friction damper, (5) electromagnetic actuator, (6) electromagnetic-actuator electrical connection, (7) mechanical support.

pulse-width modulated electric current. Thus, normal forces at the friction dampers are generated by the actuators as a function of the average electric current.

4.4. External excitation

During the experiments, the structure was subjected to base acceleration by means of the 6-DOF-2000E shaking table (model 170-131) from MOOG. The acceleration record consisted in a frequency sweep from 1/5 to 5 times the fundamental natural frequency of the structure, over 1 minute, with constant acceleration amplitude equal to 0.05 g. This type of excitation was used for two reasons: (1) it allows assessing the performance of the control system in a wide frequency range that includes the resonance; and (2) nonlinear phenomena, as the slackening of the cables, can be seen. Moreover, a variable-frequency harmonic load is qualitatively representative of vibrations induced by variable speed rotating machines; e.g. reaction wheel assemblies in space structures [5,42,43].

If the base acceleration is $\ddot{x}_g$, the external excitation forces in Eqs. (1)–(3) can be stated as:

$$F_{es}(t) = -\ddot{x}_g m_s, \quad F_{ed1}(t) = F_{ed2}(t) = -\ddot{x}_g m_d. \tag{27}$$

5. Numerical and experimental results

This section shows the numerical and experimental results for each case studied. Numerical simulations based on the mathematical model developed in Section 2 were carried out in MATLAB/Simulink using a stiff fifth-order implicit integration method with variable time step (ode15s).

5.1. Passive control

Six cases with PC were considered, in which the electromagnetic actuators apply different constant normal forces, N_i, namely: 2.0, 3.5, 7.0, 9.0, 13.0 and 15.0 N during each test; i.e. $N(t) = N_i$. For clarity, the following figures only show the response in the time period around system resonance ($\sim$ 1.7 Hz).

Fig. 8 shows displacement responses of the structure ($q_s(t)$) with PC from the experimental tests and their corresponding numerical simulations. Note the goodness of fit depends on the case; e.g., Normalized Mean Square Error [44,45] (NMSE) is 5% for $N =$ 2 N and 49% for $N = 15$ N. When cables are taut, the dissipation of energy is dominated by friction of the dampers; so the oscillation damps quickly after resonance (Fig. 8(a,b)). On the contrary, when cables get slack (phenomenon clearly seen for values of N greater than 9 N), the only source of dissipation is the internal damping of the structure; so the oscillation damps slowly after resonance from 10 s (Fig. 8(e,f)). As can be seen, slackening also deteriorates model accuracy. In the transitional cases (Fig. 8(c,d)), the cables get slack only for small displacements; this transition is explained in the Appendix.

Note that the compromise between avoiding cable slackening and applying high dissipative forces to the structure makes that the PC cases have an optimal normal force, which is such that $\mu N < k_d \Delta_0$ (to prevent the cable from slackening).

Fig. 9 shows some characteristic hysteresis loops of one of the SAFTs that were recorded during tests along with numerical simulation. The hysteresis loops resemble the classical bilinear hysteretic model [46], when the cable is taut (Fig. 9(a,b)). In other cases, forces vanish due to cable slackening (Fig. 9(d–f)). Also, it is observed that taut-cable condition (17) is only satisfied in Fig. 9(a), condition (18) is satisfied in Fig. 9(a–c) and none of them are satisfied in Fig. 9(d–f).

Fig. 9(a) and (b) show clearly a good approximation between numerical and experimental results and keep the shape of Fig. 2.

Only two differences can be seen between numerical and experimental results of Fig. 9(c–f): (1) the high frequency oscillations in cable forces (related to the subsystem: auxiliary spring-damper mass) damp faster in the experiments; and (2) there is a soft transition in the cable force when it gets taut. Since the effect of these differences is negligible in both, dissipated energy and equivalent overall stiffness of the SAFTs, it is expected that the numerical model is appropriate to predict the structural response and the mean and peak cable forces.

5.2. Semi-active control

Eight cases were considered with SAC (four for each control law), in which the controller makes the electromagnetic actuators to apply normal forces $N(t)$ that are variable between $N_{\min} = 2$ N and $N_{\max}$, which can be equal to 7, 9, 13 or 15 N, as the case may be.

Fig. 10 shows experimental and numerical results for the displacement responses of the structure ($q_s(t)$) with SAC when using the SQDCL. Lower dispersion than for PC (7% < NMSE < 11%) is displayed. Unlike the cases with PC, there is a clear trend towards displacement reduction as $N_{\max}$ increases.

Fig. 11 shows some characteristic hysteresis loops of one of the SAFTs that were recorded during tests with SAC using the SQDCL. It can be observed that enclosed area and peak forces fit acceptably (which are important for performance prediction and cable design). The shape similarity between Fig. 11(a–d) and Fig. 3 validate assumptions made in Section 3. The main difference between these hysteresis loops and those corresponding to PC is that dissipative forces increase with the normal force, while avoiding cable

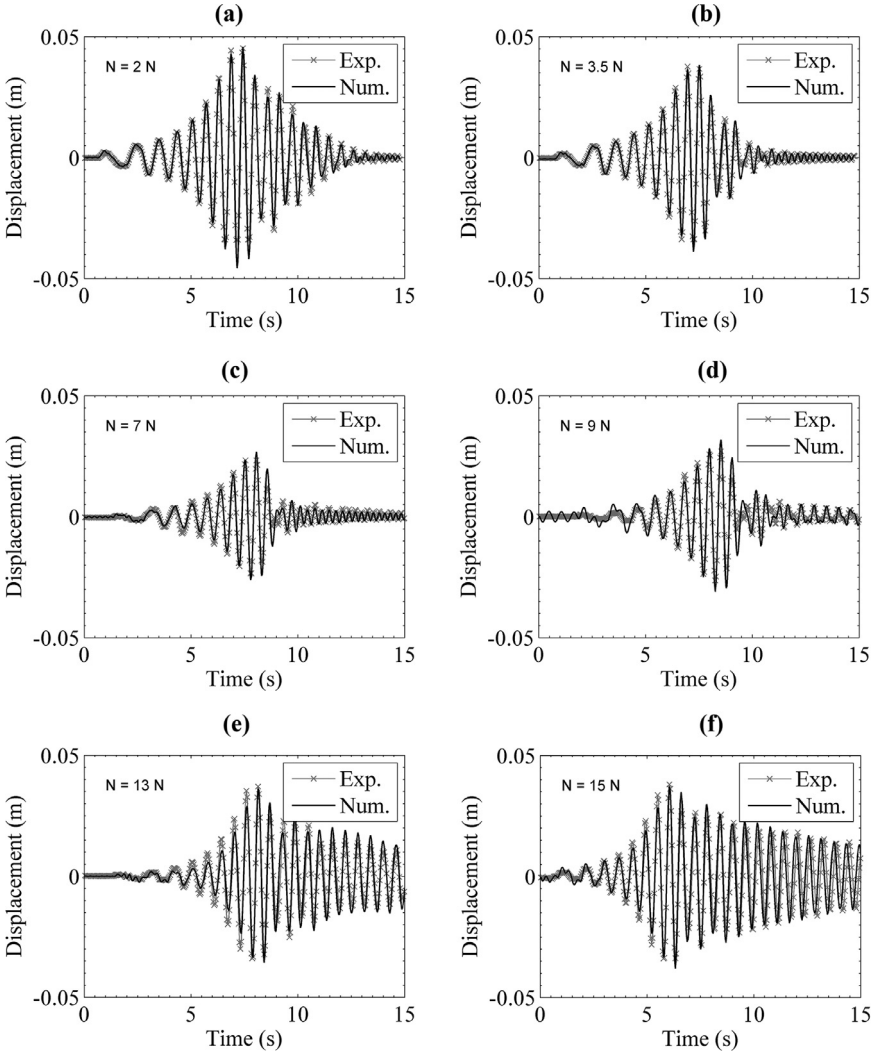

Fig. 8. Structure displacement history with PC.

slackening. This is because taut-cable conditions (21) and (22) are satisfied in all the cases shown in Fig. 11, unlike taut-cable conditions (17) and (18) which are not satisfied in all the cases of Fig. 9.

The particular case shown in Fig. 11(e), in which displacements and forces were acquired after 15 s (see Fig. 10), demonstrates that, with the SQDCL, the SAFTs dissipate energy even if the maximum displacement is very small (e.g. $\pm$ 1 mm). The enclosed area becomes quasi-triangular because of the resetting stiffness phenomenon [31,32,40,41]. That phenomenon is also present for large displacement, which can be seen as abrupt unloading branches in Fig. 11(a–d). However, its influence is bigger when the displacements are so small that the cable is unloaded before friction can occur; in this regard, Fig. 11(e) evidences that resetting stiffness implies energy dissipation without friction. The noticeable differences (oscillations along the displacement axis) between experimental and numerical curves in Fig. 11(e) are mainly due to small vibrations of the L-shaped supports shown in Fig. 6(a).

Fig. 12 shows experimental and numerical results for the displacement responses of the structure ($q_s(t)$) with SAC when using the SPCL. In this case a better fit and lower dispersion ($5\% < \text{NMSE} < 22\%$) than for PC is observed. Similar to the cases with the SQDCL, irreversible slackening is not present and there is a clear tendency towards displacement reduction as $N_{\max}$ increases. Moreover, the achieved displacement reduction is superior to that with the SQDCL (compare Fig. 12(d) to Fig. 10(d)).

Fig. 13(a–d) shows some characteristic hysteresis loops of one of the SAFTs that were recorded during the tests of SAC with the SPCL (note the good agreement with numerical simulations for enclosed areas and peak forces). Similar to the case of the SQDCL, the dissipative forces increase with the normal force while avoiding cable slackening. Assuming the same maximum displacement and maximum normal force, the enclosed area reached with SPCL is larger than with SQDCL (see Fig. 11) because the cable force reaches lower values in the backward-friction branch. Another important difference is present in the unloading branches, which are abrupt in the case of the SQDCL and have a slope approximately equal to the cable stiffness in the case of the SPCL. By comparison with analytically constructed hysteresis loops, it also observed that the shape shown in Fig. 13(a) is similar to that shown in Fig. 4(c), the shapes shown in Fig. 13(b,c) are similar to that shown in Fig. 4(b), and the shape shown in Fig. 13(d) is similar to that shown in Fig. 5; except for the oscillations, which do not substantially modify the enclosed area. This validates the assumptions made in Section 3.

Fig. 13(e) demonstrates (with displacements and forces acquired after 15 s), the hysteresis loop degenerates into a straight line with no enclosed area for very small displacements. This is

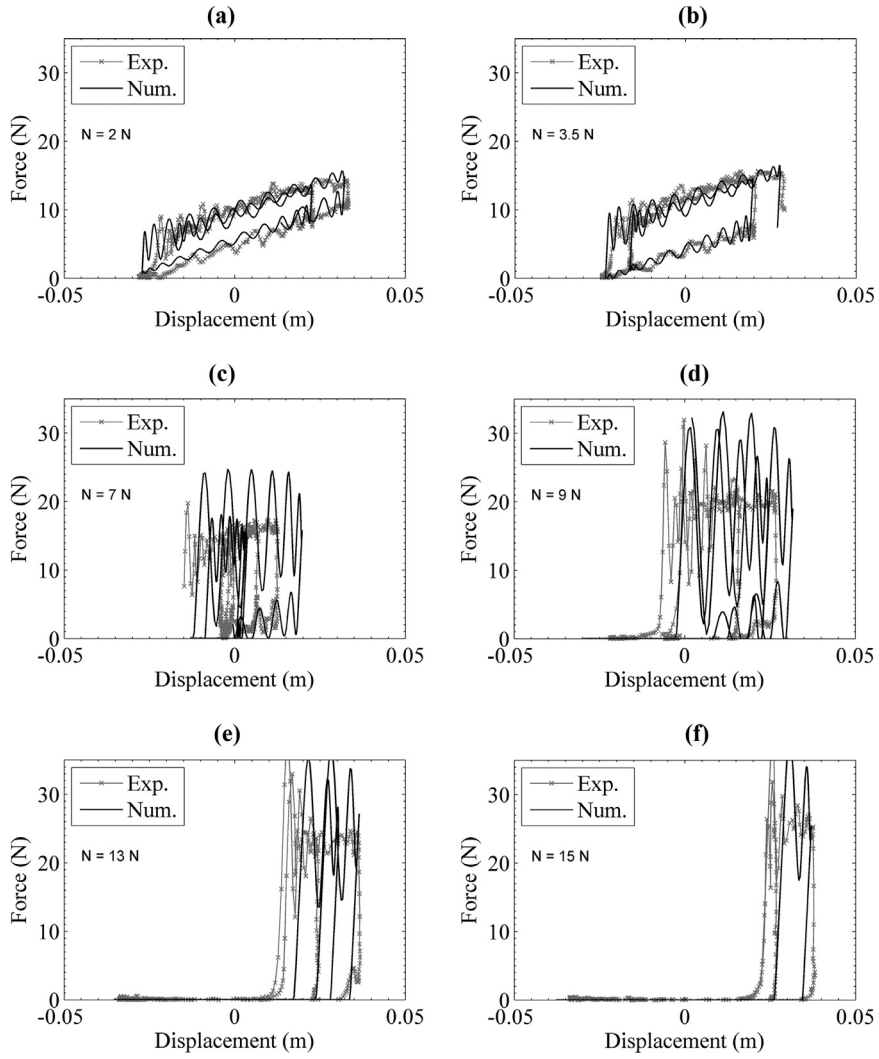

Fig. 9. Hysteresis loops with PC.

clearer in the numerical results which neglect the small vibrations of the L-shaped supports.

6. Effectiveness results and discussion

6.1. Large displacements

6.1.1. Definition of effectiveness indexes

To quantify the effectiveness of the control systems in terms of displacement reduction, the following two classical performance indexes are used [47]:

$$J_{peak} = \frac{\max\limits_{j=1,M} \left|q_{s(C)}(j\Delta_t)\right|}{\max\limits_{j=1,M} \left|q_{s(NC)}(j\Delta_t)\right|}; \tag{28}$$

$$J_{rms} = \sqrt{\frac{\sum_{j=1,M}^{M} \left|q_{s(C)}(j\Delta_t)\right|^2}{\sum_{j=1,M}^{M} \left|q_{s(NC)}(j\Delta_t)\right|^2}}; \tag{29}$$

In Eqs. (28) and (29): $\Delta_t M$ is the test duration; $q_{s(C)}(t)$ is the displacement response of the structure with PC or SAC, as the case may be; and $q_{s(NC)}(t)$ is the displacement response of the structure without control. In this last case, the structural response was obtained under the same base excitation (Section 4.4) numerically, by using Eq. (1) with $F_{c1} = F_{c2} = 0$; and experimentally, by removing both cables.

6.1.2. Effectiveness and dissipated energy

Fig. 14 shows the previously defined effectiveness indexes for the three studied cases. As can be seen, both, the peak- and RMS-displacements, are drastically reduced as compared to the uncontrolled case ($J_{rms} = J_{peak} = 1$). It is noticeable that, despite the values of NMSE (4% ~ 49%), effectiveness indexes have small errors (1 ~ 10% for most cases and 20% in the worst).

For PC, the effectiveness indexes have an optimum normal force $N = 7$ N. For SAC with the SQDCL, the effectiveness indexes decrease linearly with N_{max}; whereas with the SPCL, the effectiveness indexes decrease showing an approximately parabolic dependence on N_{max}. It is evident that the achievable effectiveness with SAC is superior to that with PC, irrespective of the chosen control law. When comparing both control laws, it is seen that the SPCL is superior to the SQDCL for every value of N_{max}.

Fig. 15 shows the dissipated energy obtained with PC, (Eq. (19)), with SAC under the SQDCL, (Eq. (23)) and with SAC under the SPCL (Eq. (25)), generated using the system parameters defined in Section 4, and the maximum displacement chosen as the average of the displacements observed in the tests as a representative case.

Regarding PC, Fig. 15 shows that the dissipated energy increases linearly with N up to the point in which the condition (17) is not

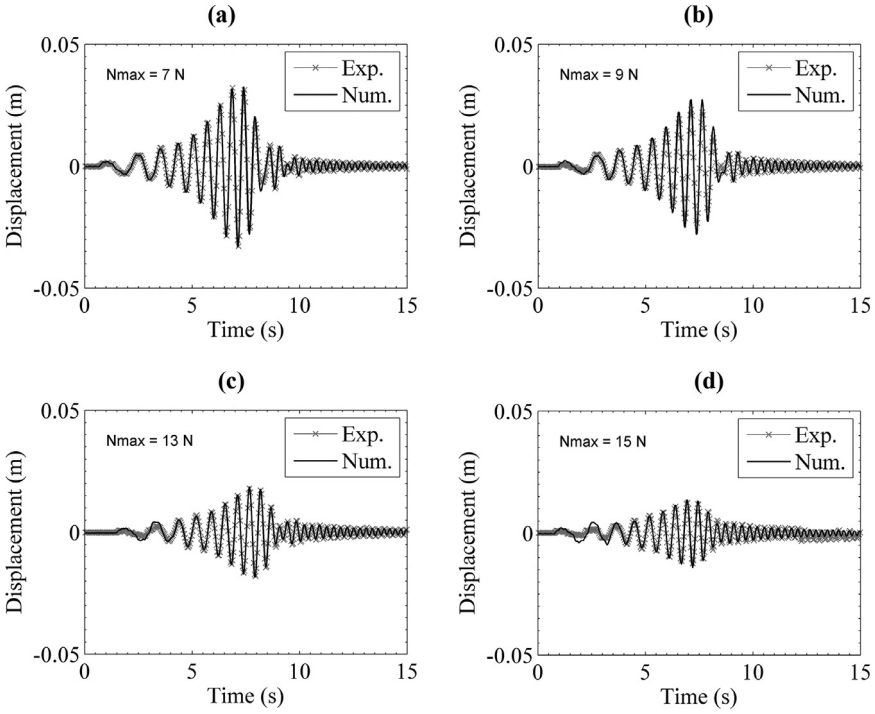

Fig. 10. Structure displacement history with SAC and the SQDCL.

satisfied (3.74 N). It is evident the existence of an optimal normal force that is between 3.74 and 7.74 N (for this example); which agrees with the effectiveness results shown in Fig. 14.

As regards SAC with the SQDCL, Fig. 15 shows that the dissipated energy increases linearly with $N_{\max}$ without restriction. Then, the achievable effectiveness with the SQDCL is always superior to that with PC (see Fig. 14). However, this increase has a slope that is a half of that of PC (in its linear part); which explains why the optimum effectiveness with PC is superior to that with the SQDCL for $N_{\max(SAC)} = N_{(PC)}$, as shown in Fig. 14.

As regards SAC with the SPCL, Fig. 15 shows that the dissipated energy increases linearly with $N_{\max}$ up to 2.74 N, with the same slope as with PC. Then, it increases parabolically up to 10.74 N. Finally, it increases linearly with the same slope as with the SQDCL without restriction. Then, for a given range of normal forces, the dissipated energy and, therefore, the achievable effectiveness with the SPCL are always superior to that with PC or with the SQDCL (as in the example shown Fig. 14).

6.2. Very small displacements

By evaluating Eqs. (20), (24) and (26) at the system parameters defined in Section 4, the following lower bounds on the maximum displacement are obtained:

$$\begin{aligned} &E_{D(PC)} = 0 \text{ if } q_{s\max} \leq 0.7 \cdot 10^{-3} \text{ m},\\ &E_{D(SQDCL)} = 0 \text{ if } q_{s\max} \leq 0.2 \cdot 10^{-3} \text{ m},\\ &E_{D(SPCL)} = 0 \text{ if } q_{s\max} \lessapprox 1.0 \cdot 10^{-3} \text{ m}. \end{aligned} \tag{30}$$

Note that (in this example) the SPCL, though more effective for large displacements, becomes ineffective if the maximum displacement is smaller than 1 mm, since the dissipated energy is null; this is clearly demonstrated in Fig. 13(e). In contrast, the SQDCL becomes ineffective only if the maximum displacement is smaller than 0.2 mm. In this regard, Fig. 11(e) shows a quasi-triangular enclosed area for a maximum displacement of 1 mm. In the case of PC, the lower bound on the maximum displacement is between the other two cases.

6.3. Robustness against pre-tension loss

A critical aspect in the reliability of any tensile system is its robustness against loss of pre-tension since this can lead to loss of effectiveness. Such a robustness can be quantified as the insensitivity of the dissipated energy E_D (which is related to the effectiveness) to changes in the pre-tension Δ_0. Although this aspect has not been addressed experimentally in this paper, numerical simulations shown in reference [33] validate the following analysis.

In Section 6.1.2, the optimum normal force μN for PC was proved to be between $k_d(\Delta_0 - q_{s\max})$ and $k_d\Delta_0$. Then, the energy dissipated per cycle must be calculated by means of the second piece of the function stated in Eq. (19). Evidently, the dissipated energy is sensitive to pre-tension Δ_0. The sensitivity of the dissipated energy (PC) to the pre-tension is defined as $S_{\Delta_0}^{E_{D(PC)}}$ and can be calculated by differentiating the second piece of Eq. (19) with respect to Δ_0 and normalizing, i.e.:

$$S_{\Delta_0}^{E_{D(PC)}} = \frac{\partial E_{D(PC)}}{\partial \Delta_0} \cdot \frac{\Delta_0}{E_{D(PC)}} = \frac{\Delta_0}{q_{s\max} + \Delta_0 - \frac{\mu N}{k_d}}. \tag{31}$$

For the example considered in this paper, this implies a 1.6% reduction in the dissipated energy for each 1% reduction in the pre-tension. Then, it can be stated that the optimum case of PC is not robust against loss of pre-tension. However, it must be said that some suboptimal cases can be easily proved to be robust against loss of pre-tension.

In the case of SAC with the SQDCL, by making a sensitivity analysis to Eq. (23), it can be obtained that:

$$S_{\Delta_0}^{E_{D(SQDCL)}} = \frac{\partial E_{D(SQDCL)}}{\partial \Delta_0} \cdot \frac{\Delta_0}{E_{D(SQDCL)}} = 0 \quad \text{if} \Delta_0 > \frac{\mu N_{\min}}{k_d} + q_{s\max}. \tag{32}$$

Then, the system with the SQDCL is robust against any loss of pre-tension satisfying this condition.

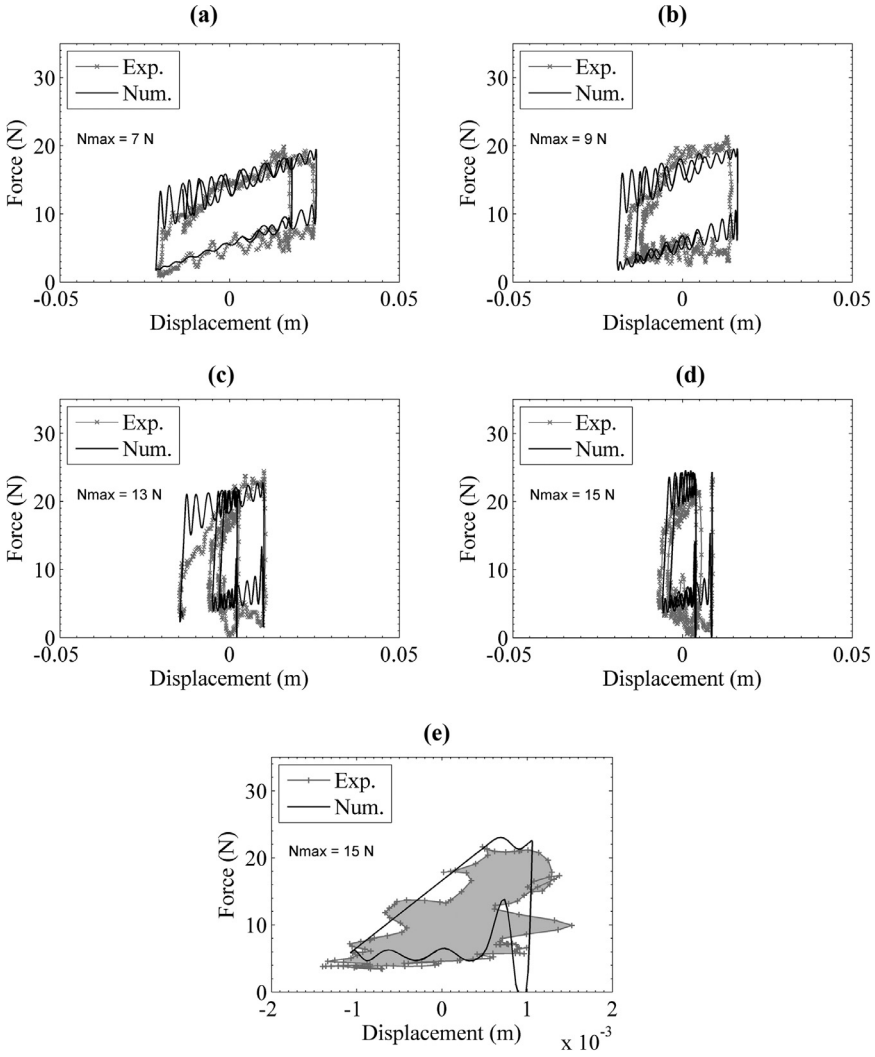

Fig. 11. Hysteresis loops with SAC and the SQDCL: (a-d) large displacements, (e) small displacements.

Similarly, for SAC with the SPCL, from the second case of Eq. (25) (which is the most efficient), it can be obtained:

$$S_{\Delta_0}^{E_{D(SPCL)}} = \frac{\partial E_{D(SPCL)}}{\partial \Delta_0} \cdot \frac{\Delta_0}{E_{D(SPCL)}} = \frac{k_d \Delta_0}{\mu N_{\max} + k_d \Delta_0 + v_F}, \tag{33}$$

which, for the example considered in this paper ($N_{\max} = 15$ N), implies a 0.3% reduction in the dissipated energy for each 1% reduction in the pre-tension. Note that, though the SPCL is not as robust as the SQDCL, it is five-fold less sensitive to loss of pre-tension than PC.

7. Conclusions

In this paper, shaking table tests, numerical simulations, and analytical developments were carried out to compare the effectiveness of proposed Semi-Active Friction Tendon (SAFTs) under passive control (PC) and semi-active control (SAC) with two different control laws, one is based on velocity-feedback (denoted as SQDCL) and the other is based on force-feedback (denoted as SPCL) .

The main conclusions of the present work are:

(1) The developed nonlinear model is accurate enough for: (1) assessing the effectiveness in displacement reduction and (2) sizing cables, anchorages and dampers.
(2) For a given pre-tension force, the achievable effectiveness with SAC is always superior to that with PC, irrespective of the chosen control law.
(3) If the displacements are so large that the deformation of cable can be neglected, the achievable effectiveness with the SPCL is always superior to that with the SQDCL.
(4) If the displacements are so small that the deformation of cable is not negligible, the SPCL can become ineffective while the SQDCL is still effective (in terms of energy dissipation). Moreover, in the ideal case in which the minimum normal force is null, the SQDCL is effective even for very small displacements.

These conclusions suggest that the SQDCL is more appropriate for applications involving stringent vibration limits, e.g. large space structures [21] or precision equipment [3]; whereas the SPCL is more appropriate where strong displacement reduction is needed only during large loads, e.g. vibration control of civil structures [1]. Evidently, SAC should be considered only if PC does not achieve the application requirements in terms of effectiveness and robustness against loss of pre-tension.

Notwithstanding these suggestions, it is remarked that the closed-form expressions derived in this paper for the “energy dissipated per cycle”, the “lower bound on the maximum displacement”, and the “sensitivity to loss of pre-tension” can be used as

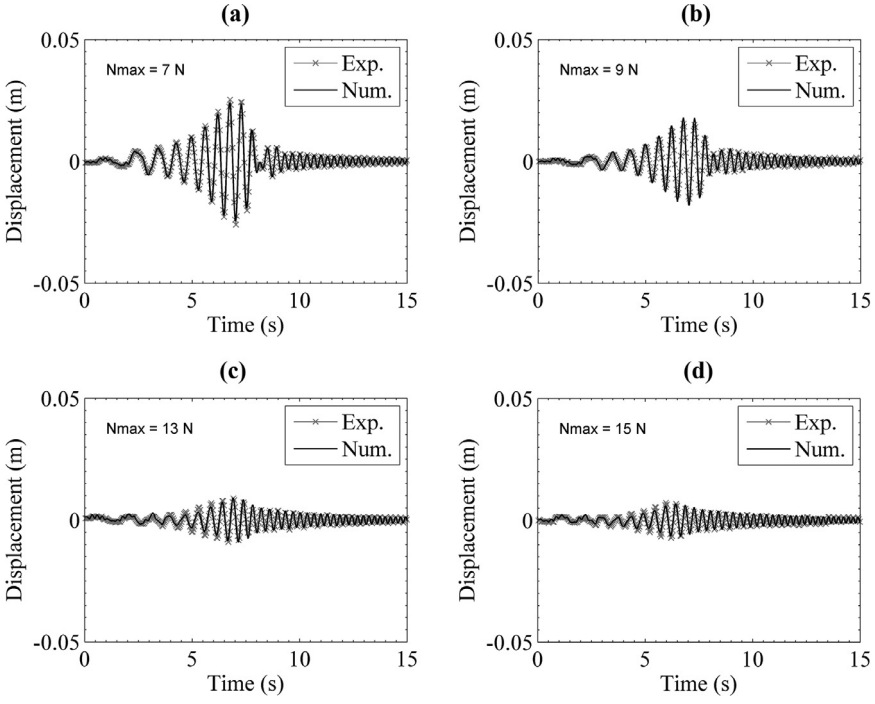

Fig. 12. Structure displacement history with SAC and the SPCL.

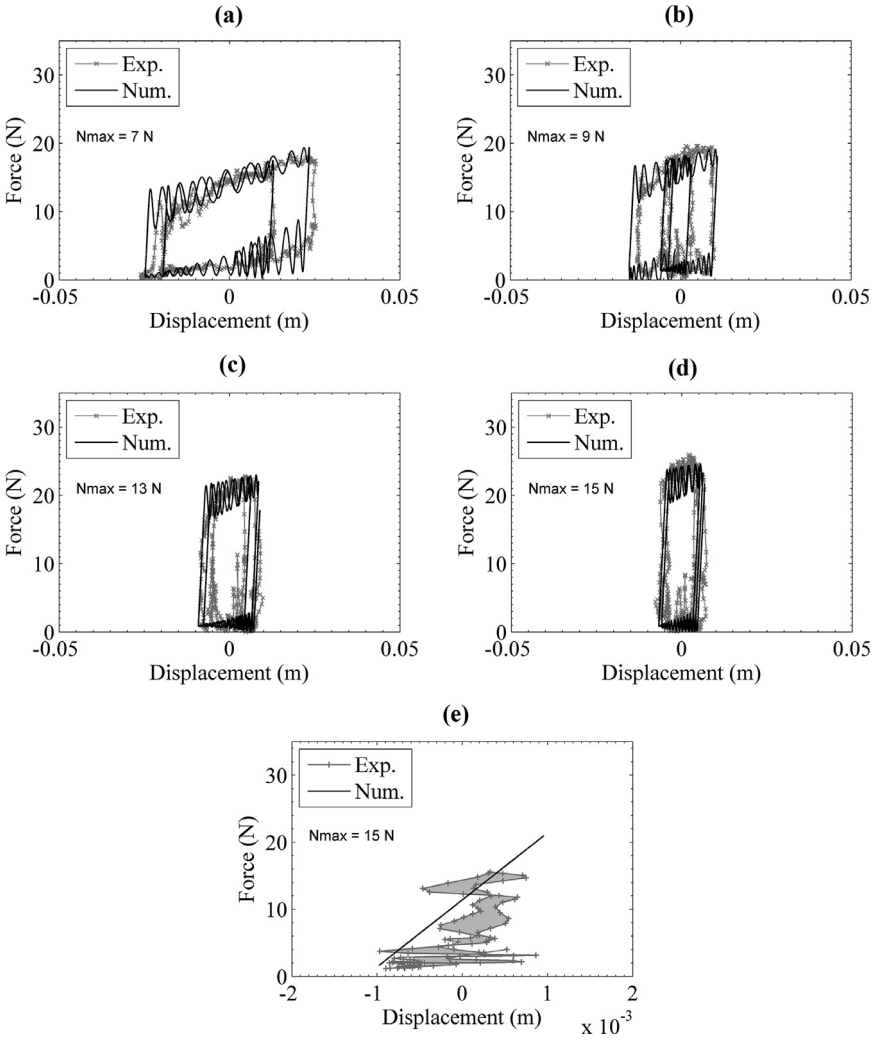

Fig. 13. Hysteresis loops with SAC and the SPCL: (a–d) large displacements, (e) small displacements.

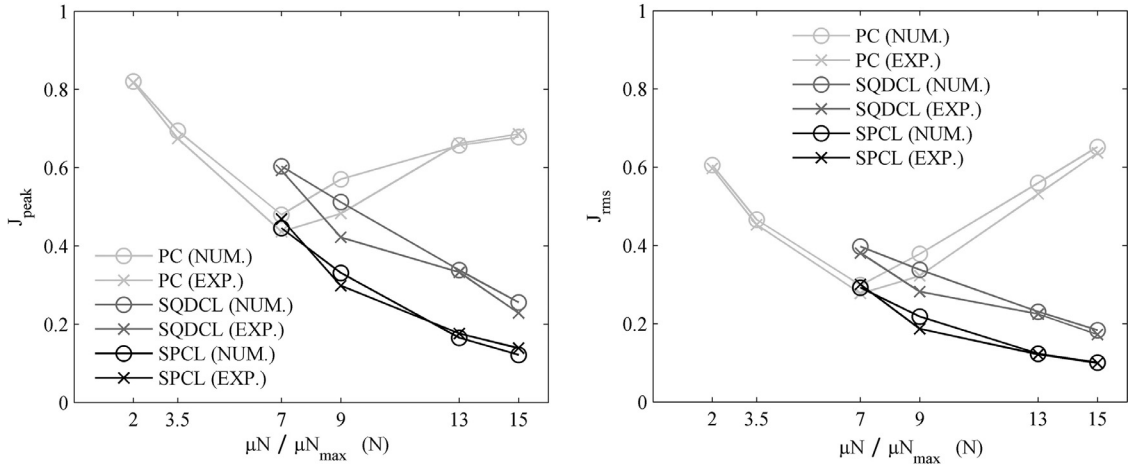

Fig. 14. Effectiveness of the control system in terms of peak and RMS displacement reduction.

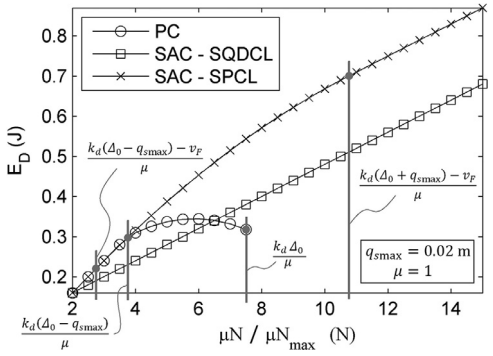

Fig. 15. Energy dissipated per cycle, for large displacements.

an engineering tool in the preliminary design of any practical application of vibration control that could use SAFTs. This includes the comparison with other alternatives, the non-trivial decision to use PC or SAC and the choice of the control law. Moreover, these closed-form expressions can be used in linearization techniques for fast response analysis.

Acknowledgements

The authors would like to thank National Research Council from Argentina (CONICET) and National University of Cuyo for the financial support. The deep examination of the reviewers is gratefully appreciated. Moreover, the help received from Eng. Gabriel Houri, during the preparation and execution of the experiments, and from Public Translator Cinthia Garrido, in the English proofread of this paper, is gratefully acknowledged.

Appendix. Derivation of expressions for dissipated energy

Generalities

A SAFT is a two-ends device in which one end is fixed and the other one has a displacement denoted as q_s. The displacement is such that $-q_{smax} \le q_s(t) \le q_{smax}$, where q_{smax} can be assumed to be externally imposed.

All analytically-constructed force/displacement diagrams (Fig. 2–5) describe a closed curve, i.e. a hysteresis loop. Fortunately, that loop can be decomposed into two functions: $F_{c+}(q_s)$ when $\dot{q}_s > 0$, and $F_{c-}(q_s)$ when $\dot{q}_s < 0$.

On this basis, the energy *supplied to* the SAFT when the displacement q_s increases from $-q_{smax}$ to q_{smax} is given by:

$$E_s = \int_{-q_{smax}}^{q_{smax}} F_{c+}(q_s)\ dq_s, \tag{A.1}$$

while the energy *returned from* the SAFT when the displacement q_s decreases from q_{smax} to $-q_{smax}$ is given by:

$$E_r = -\int_{q_{smax}}^{-q_{smax}} F_{c-}(q_s)\ dq_s. \tag{A.2}$$

Therefore, the energy that a SAFT dissipates per cycle equals to $E_D = E_s - E_r$. Thus, E_D can be obtained as the area under the force/displacement diagram [37]. In the following derivations, this area is calculated straightforwardly by adding or subtracting well-known formulae for the area of parallelograms and triangles.

Passive control

The following closed-form expression for the energy dissipated per cycle can be obtained from geometrical considerations on Fig. 2:

$$E_{D(PC)} = \frac{k_c}{k_c + k_d}\left(4q_{smax}\mu N - \frac{4(\mu N)^2}{k_c}\right)$$
$$\text{if } \mu N < k_d(\Delta_0 - q_{smax}) \text{ and } q_{smax} \ge \frac{\mu N}{k_c}. \tag{A.3}$$

Note that the first term of Eq. (A.3) accounts for the enclosed area of the parallelogram (1,2,4,5) and the second one accounts for the two missed triangles, (1,2,3) and (4,5,6), in Fig. 2.

From Eq. (A.3) can be observed that, when the maximum displacement is small, the second term is relevant respect to the first one and the energy dissipated per cycle is reduced. Evidently, by inspecting Fig. 2, the friction branches vanish if the maximum displacement reduces enough; and, therefore, the hysteresis loop degenerates into a straight line. This lower bound on the maximum displacement can be found by equating Eq. (A.3) to zero, and solving for q_{smax}, which yields:

$$E_{D(PC)} = 0 \text{ if } q_{smax} \le \frac{\mu N}{k_c}. \tag{A.4}$$

On the contrary, if the maximum displacement is large enough and $k_c \gg k_d$ then, the second term of Eq. (A.3) can be neglected and the dissipated energy can be approximated as:

$$E_{D(PC)} \approx 4q_{smax}\mu N \text{ if } \mu N < k_d(\Delta_0 - q_{smax}). \tag{A.5}$$

As expected, Eq. (19) reduces to the standard Coulomb's friction law (Eq. (A.5)) [23].

It is interesting to consider the transitional case in which it is guaranteed that the cable gets taut at least once in every cycle but it is not always taut, i.e. the condition (18) is satisfied but condition (17) is not. In this case, the dissipated energy can be approximated as:

$$E_{D(PC)} \approx \gamma \cdot 4q_{smax}\mu N \text{ if } k_d(\Delta_0 - q_{smax}) \le \mu N < k_d\Delta_0. \quad \text{(A. 6)}$$

in which γ is a reduction factor that depends on the displacement fraction in which the cable force vanishes, i.e.:

$$\gamma = \frac{1}{2} + \frac{1}{2}\left(\frac{q^*_{smax}}{q_{smax}}\right), \quad \text{(A.7)}$$

where q^*_{smax} is the larger maximum displacement that satisfies the condition (17), i.e.:

$$q^*_{smax} = \Delta_0 - \frac{\mu N}{k_d}. \quad \text{(A.8)}$$

Finally, Eqs. (A.5)–(A.8) can be combined into the following general expression of the energy dissipated per cycle for large displacements:

$$E_{D(PC)} \approx \begin{cases} 4q_{smax}\mu N & \text{if } \mu N < k_d(\Delta_0 - q_{smax}) \\ 2q_{smax}\mu N + 2\mu N\Delta_0 - \dfrac{2(\mu N)^2}{k_d} & \text{if } k_d(\Delta_0 - q_{smax}) \le \mu N < k_d\Delta_0 \end{cases} \quad \text{(A.9)}$$

Eq. (A.9) is not defined when condition (18) is not satisfied. However, that is an impractical case in which the cable does not get taut at least once and should be avoided by design, since $E_{D(PC)} = 0$.

Semi-active control with SQDCL

Analogously to the PC case, the following closed-form expression can be obtained for the energy dissipated per cycle from Fig. 3:

$$E_{D(SQDCL)} = \frac{k_c}{k_c + k_d}\left(4q_{smax}\mu N_{min} - \frac{4(\mu N_{min})^2}{k_c}\right) + \frac{k_c}{k_c + k_d}\mu(N_{max} - N_{min}) \times \left(2q_{smax} - \frac{2\mu N_{min}}{k_c} - \frac{\mu(N_{max} - N_{min})}{2k_c}\right)$$

$$\text{if } \mu N_{min} < k_d(\Delta_0 - q_{smax}) \text{ and } q_{smax} \ge \frac{\mu(N_{max} + N_{min})}{2k_c} \quad \text{(A.10)}$$

Note that the first term in Eq. (A.10) is a merely passive dissipation of energy due to the area enclosed by the points (1,3,7,9) in Fig. 3. In contrast, the second term accounts for the energy dissipated because of SAC; i.e. the area enclosed by the points (3,5,6,7). The area of the polygon (3,5,6,7) is obtained by subtracting the area of the triangle (3,4,5) from that of the parallelogram (3,4,6,7).

If the maximum displacement is small enough to make the forward-friction branch vanish, i.e. if $2q_{smax} \le \mu(N_{max} + N_{min})/k_c$, the hysteresis loop degenerates into a triangle mounted over a parallelogram (similar to the case shown in Fig. 11(e)) and the dissipated energy results:

$$E_{D(SQDCL)} = \frac{k_c}{k_c + k_d}\left(4q_{smax}\mu N_{min} - \frac{4(\mu N_{min})^2}{k_c}\right) + \frac{k_c}{k_c + k_d}\left(2q_{smax} - \frac{2\mu N_{min}}{k_c}\right)^2\frac{k_c}{2}$$

$$\text{if } \mu N_{min} < k_d(\Delta_0 - q_{smax}) \text{ and } q_{smax} \le \frac{\mu(N_{max} + N_{min})}{2k_c}. \quad \text{(A.11)}$$

Now, if the maximum displacement is small enough to make both friction branches vanish, the hysteresis loop degenerates into a straight line. This lower bound on the maximum displacement can be found by equating Eq. (A.11) to zero, and solving for q_{smax}, which yields:

$$E_{D(SQDCL)} = 0 \text{ if } q_{smax} \le \frac{\mu N_{min}}{k_c}. \quad \text{(A.12)}$$

This lower bound on the maximum displacement (with no dissipation of energy) is closely related to the passive dissipation of energy.

In the opposite situation, if the maximum displacement is large enough and $k_c \gg k_d$, the dissipated energy can be approximated, from Eq. (A.10), as:

$$E_{D(SQDCL)} \approx 2q_{smax}\mu(N_{max} + N_{min}) \text{ if } \mu N_{min} < k_d(\Delta_0 - q_{smax}). \quad \text{(A.13)}$$

Semi-active control with SPCL

In this case, as the hysteresis loops stabilize after many cycles depending on the parameters combination, it is appropriate to separate the analysis into large displacements (Fig. 4(a–c)) and very small displacements (Fig. 5).

Analogously to previous cases, when the maximum displacement is large enough and $k_c \gg k_d$, the energy dissipated per cycle can be approximated by geometry from those three cases shown in Fig. 4(a–c) as follows:

$$E_{D(SPCL)} \approx \begin{cases} 4\mu N_{max}q_{smax} & \text{if } \mu N_{max} \le k_d(\Delta_0 - q_{smax}) - v_F, \\ 2q_{smax}(\mu N_{max} + k_d\Delta_0 - v_F) & \text{if } \mu N_{max} \ge k_d(\Delta_0 + q_{smax}) - v_F \\ 4\mu N_{max}q_{smax} & \text{elsewhere} \\ \quad - \dfrac{(\mu N_{max} - k_d(\Delta_0 - q_{smax}) + v_F)^2}{2k_d} & \end{cases}$$

$$\text{if } \mu N_{min} < k_d(\Delta_0 - q_{smax}) - v_F. \quad \text{(A.14)}$$

Unlike the previous case, N_{min} does not appear in the three cases of Eq. (A.14) and it is observed a detrimental effect of high values of v_F in two of them.

Now consider the case shown in Fig. 5 in which the maximum displacement is small enough to neglect the variable component of auxiliary spring force, $k_d q_s$, in friction branches, but not the effect of cable stiffness in loading and unloading branches. In this case, the unloading branch (3-4) has a slope equal to the cable stiffness because the SPCL switches the normal force from N_{max} to N_{min} just when the cable force reaches the force threshold, v_F (point 4 of Fig. 5).

By inspecting Fig. 5, it is evident that the hysteresis loop degenerates into a straight line if the displacement is so small that both friction branches vanish. This lower bound of the maximum displacement changes every cycle until it converges to a value that can be approximated as follows (see Fig. 13(e)):

$$E_{D(SPCL)} = 0 \text{ if } q_{smax} \lessapprox \frac{\mu N_{max} + k_d\Delta_0 - v_F}{2k_c}. \quad \text{(A.15)}$$

References

[1] Preumont A, Seto K. Active control of structures. Chichester, UK: John Wiley & Sons; 2008.

[2] Spelta C, Previdi F, Savaresi SM, Fraternale G, Gaudiano N. Control of magnetorheological dampers for vibration reduction in a washing machine. Mechatronics 2009;19:410–21. doi:10.1016/j.mechatronics.2008.09.006.

[3] Rivin EI. Vibration isolation of precision equipment. Precis Eng 1995;17:41–56. doi:10.1016/0141-6359(94)00006-L.

[4] Su YX, Duan BY, Wei Q, Nan RD, Peng B. The wind-induced vibration control of feed supporting system for large spherical radio telescope using electrorheological damper. Mechatronics 2003;13:95–110. doi:10.1016/S0957-4158(01)00042-3.

[5] Preumont A. Vibration control of active structures: an introduction. 3rd ed. Netherlands, Dordrecht: Springer; 2011. doi:10.1007/978-94-007-2033-6.
[6] Hurlebaus S, Gaul L. Smart structure dynamics. Mech Syst Signal Process 2006;20:255–81. doi:10.1016/j.ymssp.2005.08.025.
[7] Soong TT, Dargush GF. Passive energy dissipation systems in structural engineering. Chichester, UK: John Wiley & Sons; 1997.
[8] Casciati F, Rodellar J, Yildirim U. Active and semi-active control of structures - theory and applications: a review of recent advances. J Intell Mater Syst Struct 2012;23:1181–95. doi:10.1177/1045389×12445029.
[9] Lackner MA, Rotea MA. Structural control of floating wind turbines. Mechatronics 2011;21:704–19. doi:10.1016/j.mechatronics.2010.11.007.
[10] Lim CW. Active vibration control of the linear structure with an active mass damper applying robust saturation controller. Mechatronics 2008;18:391–9. doi:10.1016/j.mechatronics.2008.06.006.
[11] Palacios-Quiñonero F, Rubió-Massegú J, Rossell JM, Karimi HR. Vibration control for adjacent structures using local state information. Mechatronics 2014;24:336–44. doi:10.1016/j.mechatronics.2013.08.001.
[12] Gawronski W. Advanced structural dynamics and active control of structures. New York: Springer; 2004.
[13] Savaresi SM, Poussot-Vassal C, Spelta C, Sename O, Dugard L. Semi-active suspension control design for vehicles. Amsterdam - Boston - Heidelberg - London - New York - Oxford Paris - San Diego - San Francisco - Singapore - Sydney - Tokyo: Elsevier; 2010.
[14] Garrido H, Curadelli O, Ambrosini D. A straightforward method for tuning of Lyapunov-based controllers in semi-active vibration control applications. J Sound Vib 2014;333:1119–31.
[15] Karnopp D, Crosby MJ, Harwood RA. Vibration control using semi-active force generators. ASME J Ind 1974;96:619–26.
[16] Casciati F, Magonette G, Marazzi F. Technology of semiactive devices and applications in vibration mitigation. Chichester, UK: John Wiley & Sons, Ltd; 2006. doi:10.1002/0470022914.
[17] Poussotvassal C, Sename O, Dugard L, Gaspar P, Szabo Z, Bokor J. A new semi-active suspension control strategy through LPV technique. Control Eng Pract 2008;16:1519–34. doi:10.1016/j.conengprac.2008.05.002.
[18] Luu M, Martinez-Rodrigo MD, Zabel V, Könke C. Semi-active magnetorheological dampers for reducing response of high-speed railway bridges. Control Eng Pract 2014;32:147–60. doi:10.1016/j.conengprac.2014.08.006.
[19] Lizell M. An actuator for semi-active damping system. Mechatronics 1994;4:207–15. doi:10.1016/0957-4158(94)90044-2.
[20] Hogsberg J, Brodersen ML. Hybrid viscous damper with filtered integral force feedback control. J Vib Control 2014. doi:10.1177/1077546314543912.
[21] Balas MJ. Trends in large space structure control theory: fondest hopes, wildest dreams. IEEE Trans Automat Control 1982;27:522–35. doi:10.1109/TAC.1982.1102953.
[22] Tibert G. Deployable Tensegrity Structures for Space Applications. Royal Institute of Technology; 2002.
[23] Den Hartog JP. Mechanical vibrations. 4th ed. New York: Dover Publications, Inc.; 1985.
[24] Pekcan G, Mander JB, Chen SS. Experiments on steel MRF building with supplemental tendon system. J Struct Eng 2000;126:437–44.
[25] Mualla IH, Belev B. Performance of steel frames with a new friction damper device under earthquake excitation. Eng Struct 2002;24:365–71. doi:10.1016/S0141-0296(01)00102-X.
[26] Achkire Y, Bossens F, Preumont A. Active damping and flutter control of cable-stayed bridges. J Wind Eng Ind Aerodyn 1998;74–76:913–21.
[27] Guo T, Liu Z, Cai L. An improved force feedback control algorithm for active tendons. Sensors 2012;12:11360–71. doi:10.3390/s120811360.
[28] Smrz M, Bastaits R, Preumont A. Active damping of the camera support mast of a Cherenkov Gamma-ray telescope. Nucl Instrum Methods Phys Res Sect A 2011;635:44–52. doi:10.1016/j.nima.2011.01.092.
[29] Wang Z, Li T, Cao Y. Active shape adjustment of cable net structures with PZT actuators. Aerosp Sci Technol 2013;26:160–8. doi:10.1016/j.ast.2012.03.001.
[30] Korkmaz S. A review of active structural control: challenges for engineering informatics. Comput Struct 2011;89:2113–32.
[31] Klein RE, Healey MD. Semi-active control of wind induced oscillations in structures. In: Leipholz HHE, editor. Second international symposium structural control. Ontario, Canada: Martinus Nijhoff Publishers; 1985. p. 354–69.
[32] Erramouspe J, Kiousis P, Christenson R, Vincent T. A resetting stiffness dynamic controller and its bench-scale implementation. Eng Struct 2007;29:2602–10. doi:10.1016/j.engstruct.2007.01.014.
[33] Garrido H, Curadelli O, Ambrosini D. Semi-active friction tendons for vibration control of space structures. J Sound Vib 2014;333:5657–79. doi:10.1016/j.jsv.2014.06.018.
[34] Ajrab JJ, Pekcan G, Mander JB. Rocking wall-frame structures with supplemental tendon systems. J Struct Eng 2004;130:895–903.
[35] J.B. Mander, G. Pekcan, S.S. Chen, Antiseismic device for buildings and works of art, US 6,256,943 B1, 2001.
[36] Jansen LM, Dyke SJ. Semiactive control strategies for MR dampers: a comparative study. J Eng Mech 2000;126:795–803. doi:10.1061/(ASCE)0733-9399(2000)126:8(795).
[37] Clough RW, Penzien J. Dynamics of structures. 3rd ed. Berkeley, CA 94704 USA: Computers & Structures, Inc.; 1995.
[38] Unsal M. Force control of a new semi-active pieozoelectric-based friction damper. University of Florida; 2002.
[39] Kuehn JL, Stalford HL. Stability of a Lyapunov controller for a semi-active structural control system with nonlinear actuator dynamics. J Math Anal Appl 2000;251:940–57. doi:10.1006/jmaa.2000.7177.
[40] Chase J, Mulligan K, Gue A, Alnot T, Rodgers G, Mander J, et al. Re-shaping hysteretic behaviour using semi-active resettable device dampers. Eng Struct 2006;28:1418–29. doi:10.1016/j.engstruct.2006.01.011.
[41] Lu L-Y, Lin G-L. Improvement of near-fault seismic isolation using a resettable variable stiffness damper. Eng Struct 2009;31:2097–114. doi:10.1016/j.engstruct.2009.03.011.
[42] Neat GW, Abramovici A, Goullioud R, Korechoff RP, Calvet RJ, Joshi SS. Overview of the microprecision interferometer testbed, Pasadena; 1998.
[43] Zhou W-Y, Li D-X. Design and analysis of an intelligent vibration isolation platform for reaction/momentum wheel assemblies. J Sound Vib 2012;331:2984–3005. doi:10.1016/j.jsv.2012.02.018.
[44] Walpole R, Myers R, Myers S, Ye K. Probability and statistics for engineers and scientists. 9th ed. Boston: Prentice Hall; 2012.
[45] Mohammad KS, Worden K, Tomlinson GR. Direct parameter estimation for linear and non-linear structures. J Sound Vib 1992;152:471–99.
[46] Caughey TK. Sinusoidal Excitation of a system with bilinear hysteresis. J Appl Mech 1960;27:640. doi:10.1115/1.3644075.
[47] Spencer BF, Dyke SJ, Deoskar HS. Benchmark problems in structural control: part I—active mass driver system. Earthq Eng Struct Dyn 1998;27:1127–39. doi:10.1002/(SICI)1096-9845(1998110)27:11⟨1127::AID-EQE774⟩3.0.CO;2-F.